PAPER

Decay properties of the 3_1^- level in ^{96}Mo

IOP Publishing Journal of Physics G: Nuclear and Particle Physics

J. Phys. G: Nucl. Part. Phys. **46** (2019) 075101 (16pp) https://doi.org/10.1088/1361-6471/ab0b5e

Decay properties of the 3_1^- level in ^{96}Mo

E T Gregor[1,2,15], N N Arsenyev[3], M Scheck[1,2], T M Shneidman[3,4], M Thürauf[5], C Bernards[6], A Blanc[7], R Chapman[1,2], F Drouet[8], A A Dzhioev[3], G de France[9], M Jentschel[7], J Jolie[10], J M Keatings[1,2], Th Kröll[5], U Köster[7], R Leguillon[11], K R Mashtakov[1,2], P Mutti[7], D O'Donnell[1,2], C M Petrache[11], G S Simpson[8], J Sinclair[1,2], J F Smith[1,2], T Soldner[7], P Spagnoletti[1,2], A V Sushkov[3], W Urban[7,12], A Vancraeyenest[7], J R Vanhoy[13], V Werner[5,6], K O Zell[10] and M Zielińska[14]

[1] School of Computing, Engineering & Physical Sciences, University of the West of Scotland, Paisley PA1 2BE, United Kingdom
[2] SUPA, Scottish Universities Physics Alliance, United Kingdom
[3] Bogoliubov Laboratory of Theoretical Physics, Joint Institute for Nuclear Research, 141980 Dubna, Moscow region, Russia
[4] Kazan Federal University, Kazan 420008, Russia
[5] Institut für Kernphysik, Technische Universität Darmstadt, D-64289 Darmstadt, Germany
[6] WNSL, Wright Nuclear Structure Laboratory, Yale University, New Haven CT 06520-8120, United States of America
[7] ILL, Institut Laue-Langevin, F-38042 Grenoble Cedex, France
[8] LPSC, UJF Grenoble I, F-38026 Grenoble Cedex, France
[9] GANIL, Grand Accélérateur National d'Ions Lourds, F-14076 Caen, France
[10] Institut für Kernphysik, Universität zu Köln, D-50937 Köln, Germany
[11] CSNSM, Université Paris Sud and CNRS/IN2P3, F-91405 Orsay, France
[12] Faculty of Physics, University of Warsaw, PL-00-681 Warsaw, Poland
[13] Department of Physics, United States Naval Academy, Annapolis, MD 21402-5026, United States of America
[14] IRFU, CEA, Université Paris-Saclay, F-91191 Gif-sur-Yvette, France

E-mail: eleonora.gregor@lnl.infn.it

Received 14 January 2019, revised 19 February 2019
Accepted for publication 28 February 2019
Published 15 May 2019

Abstract

The first excited 3_1^- level of ^{96}Mo was investigated in a high-statistics experiment using the ^{95}Mo(n, $\gamma\gamma$) cold neutron capture reaction. The measurements used the high cold neutron flux from the research reactor at Institut Laue-Langevin and employed the highly-efficient EXILL array to detect γ-ray

[15] Present Address: Instituto Nazionale di Fisica Nucleare, Laboratori Nazionali di Legnaro, I-35020 Legnaro, Italy.

coincidences. The recorded statistics allow identification of decay branches with only a small relative intensity including the $3_1^- \rightarrow 0_{gs}^+$ $E3$ decay. With the knowledge of the newly measured branching ratio and the known $B(E3, 3_1^- \rightarrow 0_{gs}^+)$ transition probability, the lifetime of the 3_1^- level was determined and, subsequently, the $B(E1)$ strength of the other decay branches of the 3_1^- octupole phonon were calculated. The extracted electromagnetic decay strengths are compared to the systematics of the stable even–even molybdenum isotopes and values calculated in a Skyrme-force based quasi-particle random phase approximation and in a cluster approach. Additionally, the $3_1^- \rightarrow 2_{iv}^+$ decay branch to the low-lying 2_{iv}^+ quadrupole isovector level was observed.

Keywords: octupole phonon, weak $E3$ branch, cold neutron capture reaction, QRPA calculations, cluster model calculations

(Some figures may appear in colour only in the online journal)

1. Introduction

The formation of low-lying collective excitations in the nuclear many-body quantum system has remained a very interesting research topic throughout the history of nuclear structure physics. Of particular interest is the formation of these collective excitations, which can be described within the framework of the nuclear shell structure and the associated residual forces. Gross features, such as level sequence patterns led to the development of simple collective models such as the vibrational model for spherical nuclei [1]. However, the observation of more details of these levels, especially electromagnetic transition rates [2] and g factors [3], requires a refinement of these rather crude approximations or even a complete rethinking. This necessitates the understanding of the formation of collective structures on a microscopic basis.

Nuclei in the mass region of ^{96}Mo exhibit several interesting features such as shape (or at least configuration) coexistence [4]. In the zirconium isotopes $^{90-98}$Zr ($N = 50$–58) the ground state has a spherical configuration while from ^{100}Zr ($N = 60$) the ground state starts having considerable quadrupole correlations. Recently, the observed behavior has been explained within the context of type-II shell evolution [5, 6]. This explanation considers the change of subshell structure for excited states via the tensor force, due to changed occupation probabilities of subshells. While observables such as the 2_1^+ excitation energy or the $B(E2, 0_1^+ \rightarrow 2_1^+)$ excitation probability in the Zr isotopes ($Z = 40$) show a sudden change at $N = 60$, the situation in the molybdenum ($Z = 42$) isotopic chain is different. The observables exhibit a smooth shape transition, which corresponds to spherical and γ-soft quadrupole-deformed structures. The mean-field part of the calculations in [7, 8] indicate a spherical minimum for ^{94}Mo, which becomes more shallow for ^{96}Mo and allows for a degree of γ-softness. For ^{98}Mo, the minimum is already found at a pronounced deformation in the β and γ degrees of freedom. This γ softness is noticeable in the sequence of low-lying levels below the pairing gap. In particular, the first excited 0_2^+ level provides an indication for the emerging γ softness. While for ^{94}Mo this level is found near the vibrational limit of about twice the energy of the first excited 2_1^+ level, for ^{96}Mo it is found at 1148 keV, which is just less than 1.5 times the energy of the 2_1^+ level (778 keV). In ^{98}Mo, the 0_2^+ level (735 keV) is found even below the 2_1^+ level (788 keV). Furthermore, in comparison to ^{94}Mo, ^{96}Mo exhibits

an additional 2_2^+ (1497 keV) level and a 3_1^+ (1978 keV) level, which form a band-like structure with the 4_3^+ level at 2219 keV [9]. Interestingly, a recent study using available data from particle-transfer experiments indicated that ^{96}Mo and ^{98}Mo have a similar subshell structure [10]. However, the latter study suffers from considerable systematic errors.

Another very interesting feature of the nuclei in this mass region is their enhanced octupole collectivity. In particular, ^{96}Zr exhibits a large $B(E3, 0^+ \rightarrow 3^-)$ excitation strength [11]. Inspite that a recent experiment [12] provided evidence that the $B(E3)$ strength is less than given in the compilation, it still remains comparably strong. Together with the excitation energy of the first excited 3_1^-, this $E3$ strength is the key indicator for octupole collectivity [13]. On a microscopic level, enhanced octupole collectivity is associated with the Fermi level for protons as well as neutrons that are situated between subshell combinations with a difference of total angular momentum $\Delta\ j = 3$ and orbital angular momentum $\Delta\ l = 3$. For ^{96}Mo these are the neutron (ν) $[\nu 2d_{5/2^+}, \nu 1h_{11/2^-}]_{J^\pi=3^-}$ configuration involving the partially occupied $2d_{5/2^+}$ and empty $1h_{11/2^-}$ neutron subshells and the proton (π) $[\pi 2p_{3/2^-}, \pi 1g_{9/2^+}]_{J^\pi=3^-}$ configuration involving a hole in the fully occupied $2p_{3/2^-}$ and a particle excitation into the partially occupied $1g_{9/2^+}$ subshells. Of course, these are just the major components; in the valence shell the $\Delta j = 3$, $\Delta l = 1$ neutron particle–particle $[\nu 1g_{7/2^+}, \nu 1h_{11/2^-}]_{J^\pi=3^-}$ and proton particle–hole $[\pi 2f_{5/2^-}, \pi 1g_{9/2^+}]_{J^\pi=3^-}$ excitations can also contribute. Additionally, a large number of particle–hole excitations across major shell gaps contribute to the wavefunction of the 3_1^- octupole phonon. Despite the amplitudes of the cross oscillator shell gap excitations being small, the total contribution to the excitation strength is significant [14].

A very sensitive test of the nuclear wavefunctions is the experimental observation of electromagnetic transition rate between two levels. The decay rate is linked to the reduced transition matrix elements $\langle\Psi_f||\hat{T}(\Pi L)||\Psi_i\rangle$ provided by theory. Since the electromagnetic transition operators $\hat{T}(\Pi L)$, for electric or magnetic character Π of a given transition of multipole order L, are well known, this approach represents a direct test of the wavefunctions of the initial ψ_i and final ψ_f states. In particular, electric dipole ($E1$) transitions are very sensitive to fine details of the nuclear wavefunctions (e.g. see [15]). For a pure transition, the transition matrix element entering the reduced transition probability $B(\Pi L, J_i^{\pi_i} \rightarrow J_f^{\pi_f})$ for a given transition multipolarity ΠL is connected to the experimental quantities via

$$B(\Pi L, J_i^\pi \rightarrow J_f^\pi) = \frac{1}{2J_i + 1}|\langle\Psi_f||\hat{T}(\Pi L)||\Psi_i\rangle|^2 = C_{\Pi L}\frac{I_{\rm rel}}{\tau \cdot E_\gamma^{2L+1}}. \qquad (1)$$

The factor $1/(2J_i + 1)$ considers the number of magnetic substates of the initial level, $C_{\Pi L}$ is a transition multipolarity dependent proportionality factor, and $I_{\rm rel}$ is the relative intensity of the transition. If only the γ-ray intensity is measured, it must be corrected for internal conversion. The set of required experimental observables is complemented by the lifetime τ of the initial level and the γ-ray energy E_γ to the power $2L + 1$.

In terms of transition rates, the decay of a 3_1^- level is usually dominated by fast $E1$ transitions to lower-lying 2^+ and, if present below the 3_1^- level, 3^+ and 4^+ levels. Hence, the observation of the extremely weak ground-state $E3$ transition requires very significant statistics. Consequently, the standard method of extracting $B(E3)$ strengths is Coulomb excitation [16], in which the $E3$-excitation mechanism and the $E1$-decay paths are decoupled. Exceptions are the doubly-magic ^{208}Pb nucleus [17] and the semi-magic ^{146}Gd nucleus [18], for which the 3_1^- level is the first excited level. In these cases, the $E3$ decay is the exclusive path for depopulation of the 3_1^- level. ^{96}Zr is another special case. The first excited 2_1^+ level is found astonishingly high in energy at 1750 keV, while the 3_1^- level at 1897 keV is

comparably low. Here the $1/E_{\gamma}^{2L+1}$ energy factor results in a sizable intensity for the $E3$-decay branch. However, for the vast majority of nuclei, the observation of the $E3$-decay branch to the ground state remains a challenge.

For spherical nuclei, the $B(E1,\ 3_1^- \rightarrow 2_1^+)$ strength has been shown to set the scale for the $B(E1,\ 0^+ \rightarrow 1_1^-)$ strength connecting the ground state and the spin-1 member [19] of the quadrupole–octupole coupled (QOC) $[2_1^+ \otimes 3_1^-]_{J^-}$ quintuplet [2]. Apart from doubly-magic nuclei, the QOC level is the lowest-lying 1^- excitation in a given nucleus. In a ^{96}Mo $(\vec{\gamma},\ \gamma')$ inelastic photon scattering experiment using fully polarized $\vec{\gamma}$ rays in the entrance channel, the 2795 keV candidate for a QOC 1^- level [20] has been shown to have positive parity [21]. The next lowest-lying firmly identified 1^- level (3599 keV) shows an unusual anharmonicity A:

$$A = \frac{E_{1_1^-}}{E_{2_1^+} + E_{3_1^-}} = \frac{3599\ \text{keV}}{778\ \text{keV} + 2234\ \text{keV}} \approx 1.2. \tag{2}$$

Except for nuclei near doubly-magic shell closures, it is found that $A \leqslant 1$ [20]. Indeed, two close-lying 1^- levels (3599 and 3895 keV) are observed in ^{96}Mo. From energy considerations, both are found at the sum of the 3_1^- octupole phonon (2234 keV) and the second excited 2_2^+ level (1497 keV; $A = 0.96$) and third excited 2_3^+ level (1625keV; $A = 1.01$) level, respectively.

Furthermore, in the mass region of interest, in the language of the interacting boson model (IBM) [22], strong F-vector $B(E1,\ 3_1^- \rightarrow 2_{iv}^+)$ transitions between the 3_1^- level and the 2_{iv}^+ mixed-symmetry state were observed [23]. Mixed-symmetry states represent a class of excitations for which at least one proton or neutron component in the complex wavefunction of the collective excitations is out of phase relative to the other components [24–26]. In the IBM-2, where the 2 denotes the separate treatment of proton and neutron degrees of freedom, proton and neutron bosons (pairs of two likewise nucleons) are distinguished by the F-spin quantum number. Hence, this quantum number is the boson analog to isospin for fermions. Excitations with the maximum F-spin, F_{max}, are symmetric under the exchange of protons and neutrons, while excitations with $F = F_{\text{max}} - 1$ are no longer invariant and represent mixed-symmetry excitations. In a simple two-component shell-model approach [27], it has been shown that mixed-symmetry states represent the antisymmetric and, therefore, isovector combination of the wavefunctions of the two subsystems. Due to the isovector nature, this class of states allows conclusions about the proton–neutron residual interaction. Interestingly, the above mentioned study reported an enhancement of the $E1$ transitions connecting the 3_1^- level and the 2_{iv}^+ level in comparison to the decay to the isoscalar (fully-symmetric) 2_1^+ level.

For spherical nuclei the properties of $E1$ transitions connecting low-lying levels were well explained in a microscopic study [28] using an RPA-based microscopic Q-phonon approach [29, 30].

Prior to this work, only an upper limit of $\tau_{3_1^-} > 400$ fs was known for the lifetime of the 3_1^- level in ^{96}Mo [31]. This limit was determined using the Doppler-shift attenuation method in an inelastic neutron scattering experiment [32]. From Coulomb excitation a value of $B(E3,\ 0^+ \rightarrow 3_1^-) = 0.092(12)\ \text{e}^2\text{b}^3$ [11, 33] was extracted for the $E3$-excitation strength, corresponding to a decay strength of $B(E3)\downarrow = 24(3)$ W.u. For the decay paths, four γ-ray decays as shown in figure 1 were known. Remarkably, the decays to the 2_2^+ and 2_3^+ levels are stronger by two orders of magnitude than the decay to the 2_1^+ level.

In the present work, the results of a high-statistics ^{95}Mo$(n,\ \gamma\gamma)^{96}$Mo neutron-capture experiment are reported. The new spectroscopic data links the existing experimental information and allows the lifetime of the 3_1^- level to be extracted. Hence, absolute $E1$ transition rates for the decays to lower-lying excited states are determined.

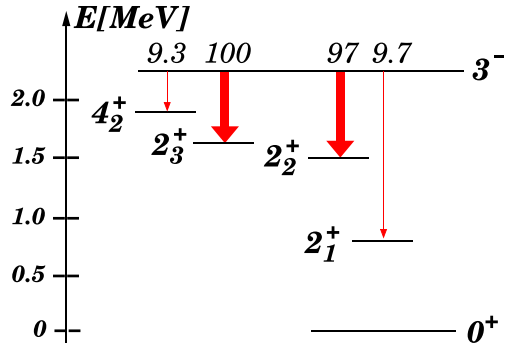

Figure 1. Partial level scheme of ^{96}Mo including the 3^-_1 level and the decays as known prior to the present work. The numbers above the arrows indicate the relative γ-ray intensity as given in the NNDC database [31].

2. Experiment: setup and data analysis

The experiment was conducted at the end of the PF1B neutron guide at the high-flux reactor at the Institut Laue-Langevin (ILL), Grenoble. The available flux of cold neutrons at the target position corresponds to a thermal neutron flux of 5×10^7 neutrons cm^{-2} s^{-1} [34]. The target consisted of 17 mg of isotopically enriched (96.47%) ^{95}Mo ($\sigma_{\mathrm{capture},n_{\mathrm{th}}} = 13.56$ b). The experience acquired in a previous (n, $\gamma\gamma$) experiment [35] has shown that for the available flux of cold neutrons a combination of neutron-capture cross section and target mass of (250 mg b) results in a count rate of ≈5000 counts s^{-1}. For this count rate the pile-up probability is low. The detector setup was part of the EXILL (EXogam at ILL) [34] (n, γ) campaign [36]. For the experiment, eight Exogam HPGe Clover detectors were available. Each Clover detector consists of four Ge crystals and was equipped with an active anti-Compton suppression shield. The detectors were mounted at a distance of 14.5 cm from the target sample at polar angles of $\theta = 90°$ with respect to the direction of the incident neutrons. An octagonal symmetry of the Clover detectors was realized for the azimuthal angles. Therefore, it was possible to have detectors at four angular groups with $\Delta\ \phi = 45°$, 90°, 135°, and 180°. In order to recover Compton-scattered events or events for which a 511 keV γ ray escaped into a neighboring crystal of the same Clover detector, an add-back procedure was applied. In the 20 hours of measuring time, a total of $3.8 \times 10^9 \gamma\gamma$-coincidence events was recorded. The events were sorted into a total $\gamma\gamma$ matrix and matrices corresponding to the four possible angular groups. In order to reduce the background events in the matrices, a second matrix was constructed for events that were not recorded within the coincidence-time window. This background matrix was subtracted from the corresponding matrix containing events registered within the coincidence-time window.

The energy calibration was made using the published results from the ^{96}Mo(n, γ) reaction [37]. Therefore, only transitions which were present as intense peaks in the spectra were employed. The low-energy part of the relative γ-ray detection efficiency $\epsilon(E_\gamma)$ was measured using a ^{152}Eu source. For the high-energy part the well-known lines emitted in the ^{35}Cl(n, γ) reaction were used [38].

In the cold neutron capture reaction, the energy of the neutron capture state (NCS) is given by the sum of the neutron separation energy of ^{96}Mo ($E_n = 9\,154.32$ keV [31]) and the negligible kinetic energy of the incident neutron. The angular momentum and parity J^π_{NCS} of the NCS is given by the $5/2^+$ ground-state spin of ^{95}Mo and the intrinsic $1/2^+$ spin of the

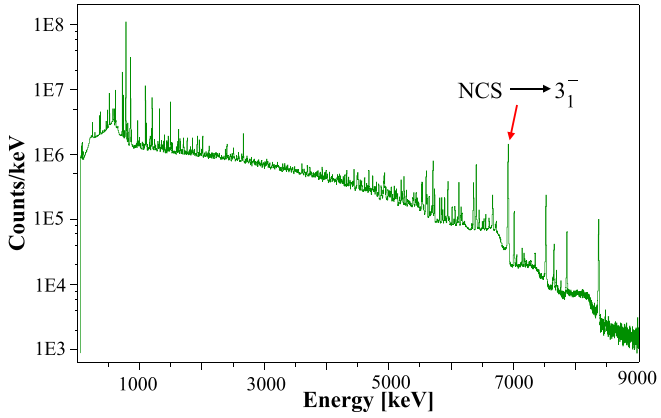

Figure 2. Projection of the total $\gamma\gamma$ matrix recorded in the ^{95}Mo(n, $\gamma\gamma$) reaction using the EXILL array. The transition connecting the neutron capture state at 9154 keV and the first excited 3_1^- level at 2234 keV is indicated. Note the log-scale of the y-axis.

incident s-wave capture neutron. Therefore, it can be expected that $J^\pi_{\rm NCS} = 2^+$ or 3^+. If $J^\pi_{\rm NCS} = 2^+$, the known $J^\pi = 1^-$ levels should be strongly populated by the preferred $E1$ transitions. However, in the $\gamma\gamma$ matrices there is no noticeable direct population of these levels from the NCS. Hence, the spin assignment of $J^\pi_{\rm NCS} = 3^+$ happens to be more likely. In any case, the 3_1^- level of interest is linked to the NCS via an $E1$ transition. Indeed, as evident in figure 2, the projection of the total $\gamma\gamma$ matrix, the transition to the 3_1^- level is the strongest decay of the NCS.

The decay of the capture state to the first excited 3_1^- level has an intensity of $N_c = 2.6 \times 10^6$ counts in the total $\gamma\gamma$ matrix. This intense transition in turn provides a formidable gate in a study of the depopulating transitions of the 3_1^- level. A spectrum resulting from this gate is shown in figure 3. Besides the previously known transitions from the 3_1^- level, two hitherto unobserved transitions are visible in the gated spectrum. The 2234 keV $E3$ transition, connecting the 3_1^- level and the ground state and the 138 keV transition to the $2^+_{4,iv}$ level (shown in the insert) are observed here for the first time. Two peaks that do not correspond to physical transitions are present in the gated spectrum at 1387 and 1525 keV. These peaks have their origin in 'true' coincidence summing due to the finite probability of two γ rays in a $\gamma\gamma$ cascade interacting with the same detector and the summing of two γ rays detected in two neighboring detector crystals in the add-back procedure. Hence, peaks, such as the one corresponding to the 3_1^- $E3$ ground-state decay, must be corrected for this summing. The probability $P_{\rm sum}(E_{\gamma_1}, E_{\gamma_2})$ for summing of an $E1$–$E2$ cascade as present for the 1387 keV peak ($3_1^- \rightarrow 2_3^+$, $E_{\gamma_1} = 609$ keV and $2_1^+ \rightarrow 0^+$, $E_{\gamma_2} = 778$ keV) and the 1525 keV peak ($3_1^- \rightarrow 2_2^+$, $E_{\gamma_1} = 737$ keV and $2_1^+ \rightarrow 0^+$, $E_{\gamma_2} = 778$ keV) is estimated as:

$$P_{\rm sum}(E_{\gamma_1}, E_{\gamma_2}) = \frac{N_{\rm sum}}{\frac{\frac{1}{2}(\epsilon(E_{\gamma_1}) + \epsilon(E_{\gamma_2}))}{\frac{N_{E_{\gamma_1}}}{\epsilon(E_{\gamma_1})} \cdot \frac{N_{E_{\gamma_2}}}{\epsilon(E_{\gamma_2})}}} \cdot Z, \tag{3}$$

where the number of counts for the summed peak, $N_{\rm sum}$, the peak intensity of γ-ray transition γ_1, N_{γ_1}, and γ-ray transition γ_2, N_{γ_2}, and the relative efficiency $\epsilon(E_{\gamma_i})$ for γ-ray detection at the respective energy enter.

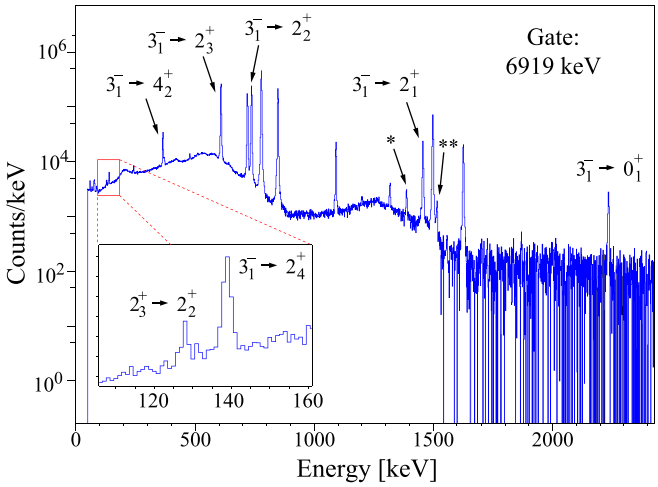

Figure 3. Spectrum gated on the 6919 keV transition populating the 3_1^- level directly from the neutron capture state. Peaks associated with transitions depopulating the 3_1^- level are labeled. The two transitions labeled with asteriks are * the 1387 keV (609 and 778 keV) and ** the 1515 keV (737 and 778 keV) sum peaks. The insert shows (in linear scale) the peak corresponding to the decay of the 3_1^- level to the $2_{4,iv}^+$ quadrupole isovector level. Unlabeled peaks correspond to the depopulation of lower-lying levels, which are fed by decays of the 3_1^- level or subsequent decays. Note the log-scale of the *y*-axis.

The factor Z

$$Z = \frac{W(\theta, J_i \to J \to J_f)}{W(\theta, J_i \to J \to J' \to J_f)} \tag{4}$$

considers the attenuation of the angular distribution [39] due to the disregarded $J \to J'$ transition in the $J_i \to J \to J' \to J_f$ three-step cascade. This procedure yields $P_{\mathrm{sum}}(609, 778) = 2.1(9) \times 10^{-7}$ and $P_{\mathrm{sum}}(737, 778) = 2.0(11) \times 10^{-7}$. In the following the error-weighted average $P_{\mathrm{sum}} = 2.06(70) \times 10^{-7}$ was used. The 3_1^- level decays via three two-step cascades with a sizeable intensity (609 and 1626 keV, 737 and 1497 keV, and 1456 and 778 keV). The contribution of these cascades to the 2234 keV peak must be considered. In this analysis, the additional contribution from summing γ-ray cascades of three γ-rays was neglected. In order to calculate the amount of counts $N_{\mathrm{sum},2234}$, for which the 2234 keV peak needs to be corrected, the following formula was applied:

$$N_{\mathrm{sum},2234} = P(E_{\gamma_1}, E_{\gamma_2}) \cdot \sum_k \left[\frac{1}{2} (\epsilon(E_{\gamma_1}) + \epsilon(E_{\gamma_2})) \frac{N_{\gamma_1}}{\epsilon(E_{\gamma_1})} \cdot \frac{N_{\gamma_2}}{\epsilon(E_{\gamma_2})} \right]. \tag{5}$$

The index k numbers the considered two-step cascades. This procedure resulted in 15% reduction of the intensity of the 2234 keV peak. Since the contribution of the summing to the other far more intense peaks is negligible their intensities were not corrected.

The γ-ray intensities extracted from the present work are given in table 1. Using the experimental branching ratio for the $3_1^- \to 0_{gs}^+$ $E3$ transition and the known $B(E3, 3_1^- \to 0^+)$ value of 24(3) W.u. [11], the half-life $T_{1/2}(3_1^-)$ of the 3_1^- level is extracted as $T_{1/2}(3_1^-) = 2.1(5) \times 10^{-12}$ s. Using this lifetime, the $B(E1)\downarrow$ values of the $E1$-decay branches given in table 1 were calculated.

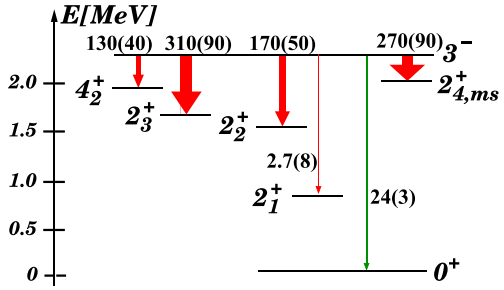

Figure 4. Decay scheme of the 3_1^- level in ^{96}Mo including the two newly observed transitions to the ground state and the $2^+_{4,ms}$ quadrupole isovector level. The $E3$ ground-state decay transition is given as a green arrow and the $E1$ decays to lower-lying excited levels as red arrows. The numbers above or next to the arrows indicate the decay strength in 10^{-6} W.u. for $E1$ transitions and W.u. for the $E3$ transition. The data are presented in table 1.

Table 1. Decay properties of the 3_1^- level in ^{96}Mo at 2234 keV as extracted from the ^{95}Mo$(n, \gamma\gamma)$ reaction. Given are the γ-ray energy E_γ, energy of the final level E_f, spin of the final level J_f, relative γ-ray intensity I_γ already corrected for internal conversion, the radiation character ΠL, and the reduced transition strength $B(EL)\downarrow$. The $B(E1)$ values were calculated using the half-life $T_{1/2}(3_1^-) = 2.1(5) \times 10^{-12}$ s, which was calculated using the known $B(E3)$ excitation strength.

E_γ (keV)	E_f (keV)	J_f	I_γ (%)	ΠL	$B(EL)\downarrow$ (W.u.)
2234	0	0^+	1.38(10)	$E3$	24(3)[a]
1456	778	2^+	12.0(6)	$E1$	$2.7(8) \times 10^{-6}$
737	1497	2^+	97(4)	$E1$	$0.17(5) \times 10^{-3}$
609	1625	2^+	100(3)	$E1$	$0.31(9) \times 10^{-3}$
365	1869	4^+	9.3(4)	$E1$	$0.13(4) \times 10^{-3}$
139	2095	2^+	1.00(7)	$E1$	$0.27(9) \times 10^{-3}$

[a] Value taken from [11].

3. Discussion

3.1. Experimental results

The decay scheme for the 3_1^- level observed in the present work is shown in figure 4. While the decays to the higher-lying 2_2^+, 2_3^+, and 4_2^+ levels exhibit $E1$-decay strengths of the order of 10^{-3} W.u., the decay to the 2_1^+ level is of the order of 10^{-6} W.u. and is consequently extremely weak. The evolution of the $3_1^- \rightarrow 2_1^+$ decay strength in the stable even–even Mo isotopes is shown in figure 5(b). While this decay in the two near-spherical isotopes ^{92,94}Mo has an $E1$ transition rate in the order of 10^{-3} W.u., the rate drops by nearly three orders of magnitude in the three isotopes ^{96,98,100}Mo. This decrease of the $3_1^- \rightarrow 2_1^+$ $E1$ strength is in contrast to the $B(E3, 3^- \rightarrow 0^+)$ strength (see figure 5(a)), which exhibits a comparably small variation. Hence, it can be concluded that the structure of the 3_1^- level changes only slightly, while the structure of the 2_1^+ level undergoes a significant change when adding a neutron pair

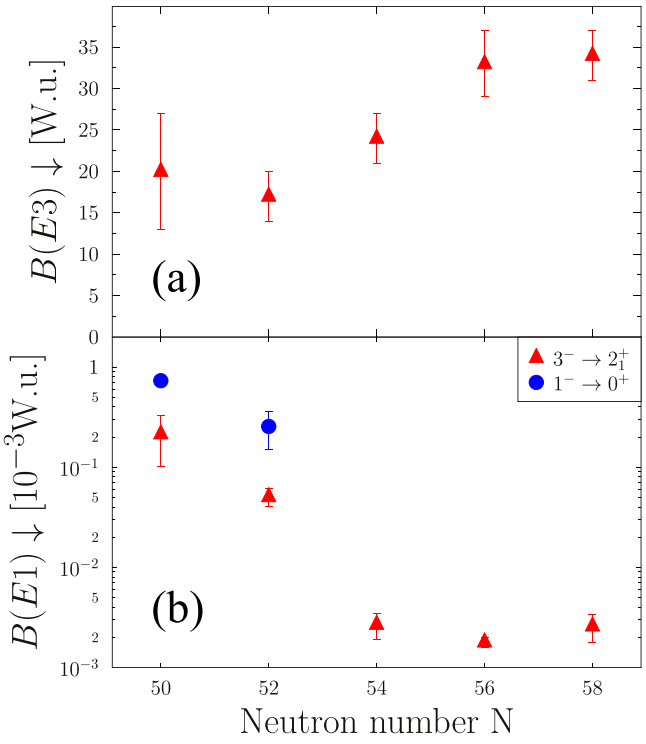

Figure 5. Experimentally observed transition rates in the stable even–even Mo isotopes. In part (a) the evolution of $B(E3, 3_1^- \rightarrow 0^+)$ strength is shown. In part (b) the $B(E1)\downarrow$ strength for the $3_1^- \rightarrow 2_1^+$ transition is given as a (red) triangle and the $1_1^- \rightarrow 0^+$ is shown as a (blue) circle. The data are taken from this work and [11, 31]. Note the logarithmic scale on the *y*-axis for part (b).

to ^{94}Mo. Indeed, an evaluation of the neutron effective single-particle energies (see figure 4(a) in [10]) exhibits a significant reduction of the subshell gap between the isolated $\nu 2d_{5/2}$ subshell and the other subshells of the valence space when moving from ^{94}Mo to ^{96}Mo. While these additional neutron configurations in the wavefunction of the 2_1^+ level do not contribute to the $B(E2, 0^+ \rightarrow 2^+)$ excitation probability (see figure 1(b) in [10]), they obviously contribute destructively to the $3_1^- \rightarrow 2_1^+$ $E1$ strength.

For ^{92,94}Mo the $B(E1, 1_1^- \rightarrow 0^+)$ reduced transition probability of the QOC 1^-level is shown in figure 5(b). The ratio R_i:

$$R_i = \frac{B(E1, 1_1^- \rightarrow 0^+)}{B(E1, 3_1^- \rightarrow 2_i^+)} \tag{6}$$

for ^{92}Mo is $R_1 = 3.4 \pm 1.9$ and for ^{94}Mo 5 ± 3 and these values are within the large quoted errors in agreement $R_1 = 7/3$ expected in a simple bosonic phonon approach [19]. Nevertheless, the two decays are of the same order of magnitude. In ^{96}Mo using the value of $B(E1, 1_1^- \rightarrow 0^+) = 0.52(12) \times 10^{-3}$ W.u. [32] of the observed 1_1^- level at 3600 keV [21] and the newly determined $B(E1, 3_1^- \rightarrow 2_1^+)$ value results in a value of $R_1 = 192.5$, which is far too high to qualify this level as a $[2_1^+ \otimes 3_1^-]_{1^-}$ QOC level. In [21] this level was already dismissed as a candidate for this kind of excitation. However, the $B(E1, 1_1^- \rightarrow 0^+)$ strength is

of the same order of magnitude as that of the $3_1^- \rightarrow 2_2^+$ decay and the ratio $R_2 = 3.1 \pm 1.6$ of these decay strengths indicates that this level is indeed rather the 1^- member of the $[2_2^+ \times 3_1^-]$ quintuplet. Based on the newly determined $B(E1, 3_1^- \rightarrow 2_1^+)$ strength, it is very likely that in ^{96}Mo the $[2_1^+ \otimes 3_1^-]_{1^-}$ QOC level is too weakly excited and, therefore, below the sensitivity limit in the previously conducted (γ, γ') experiment.

In the following, the structure of the first 3^- level in stable even–even Mo isotopes is investigated within the theoretical frameworks of the finite rank separable approximation (FRSA) and a Cluster approach. These approaches are tested against the experimental energies of the first 3^- level and the $B(E3, 3_1^- \rightarrow 0^+)$ and $B(E1, 3_1^- \rightarrow 2_1^+)$ values.

3.2. Finite rank separable approximation

3.2.1. Brief outline of the FRSA model. The FRSA has been discussed in detail in [40–42] and it is presented here briefly for completeness. The Skyrme f_- energy density functionals [43] are used for the Hartree–Fock-BCS (HF-BCS) calculations as well as for the particle–hole channel. For the interaction in the particle–particle channel, the zero-range volume force is used. The pairing strength is taken equal to -270 MeV fm^3. This value of the pairing strength is fitted to reproduce the experimental neutron pairing gaps of ^{90,92}Zr and ^{92,94}Mo obtained by the three-point formula [41, 42]. To build the quasiparticle random phase approximation (QRPA) equations on the basis of HF-BCS quasiparticle states with the residual interactions is a standard procedure [44]. The dimensions of the QRPA matrix grow rapidly with the size of the nucleus. Using the FRSA [40] for the residual interactions, the eigenvalues of the QRPA equations can be obtained as the roots of a relatively simple secular equation [41]. This procedure allows to perform QRPA calculations in very large two-quasiparticle (2QP) spaces. The cutoff of the discretized continuous part of the single-particle spectra is at the energy of 100 MeV. This is sufficient to exhaust practically the entire energy-weighted sum rule. The large configurational space renders the need for effective charges for electric transitions obsolete. Nevertheless, for $E1$ transition, the matrix elements are calculated with the effective neutron, $e_\nu^{\text{eff}} = -\frac{Z}{A}e(1 + \chi)$, and proton, $e_\pi^{\text{eff}} = \frac{N}{A}e(1 + \chi)$, charges. In the calculations bare charges $\chi = 0$ as well as quenched charges $\chi = 0.05$ and $\chi = 0.10$ were used. However, the variation of χ results in only small variations of the calculated E1 strength. Hence, the further discussion is restricted to the results with $\chi = 0$.

3.2.2. QRPA results. Calculated energies, transition probabilities, and structures of the QRPA quadrupole and octupole states of ^{92,94,96,98}Mo are given in table 2. A satisfactory description of the isotopic dependence of the 2_1^+ energies near closed shells is obtained. The closure of the neutron subshell $\nu 1g_{9/2}$ in ^{92}Mo leads to the vanishing of the neutron pairing and as a result the energy of the first 2QP pole $\{1g_{9/2}, 1g_{9/2}\}_\pi$ in ^{92}Mo is larger than the energy of the first pole $\{2d_{5/2}, 2d_{5/2}\}_\nu$ in ^{94}Mo. This yields that the 2_1^+ state has a collective structure with the domination of the proton 2QP configuration $\{1g_{9/2}, 1g_{9/2}\}_\pi$ for the case of ^{92}Mo. On the other hand, in ^{94}Mo the leading neutron configuration $\{2d_{5/2}, 2d_{5/2}\}_\nu$ gives a contribution of 66% that is approximately three times larger than in ^{96}Mo (five times when compared to ^{98}Mo). The contribution of the proton configuration $\{1g_{9/2}, 1g_{9/2}\}_\pi$ in ^{98}Mo is almost a factor two larger than in ^{94}Mo. These structural peculiarities are reflected in the $B(E2)$ values, as is shown in table 2. The $B(E2)$ strength grows with increasing neutron number. The same evolution is obtained for the $B(E3)$ strength, but the energy of the first 2QP pole, $\{1g_{9/2}, 1f_{5/2}\}_\pi$, practically remains constant with increasing neutron number. The proton 2QP-configurations exhaust about 85% of the wavefunction normalization of the 3_1^- state in ^{92}Mo, and the proton contribution to the normalization of 3_1^- state decreases towards

Table 2. Calculated energies, ground-state transition probabilities, and structures of the QRPA quadrupole and octupole states of ^{92,94,96,98}Mo. Only configurations contributing to the phonon structure with an amplitude greater than 5% are given.

	2_1^+			3_1^-		
	$E_{2_1^+}$ (MeV)	$B(E2)\downarrow$ (W.u.)	Structure $2^+_{1,\mathrm{QRPA}}$ $\%\{n_1l_1j_1, n_2l_2j_2\}_\tau$	$E_{3_1^-}$ (MeV)	$B(E3)\downarrow$ (W.u.)	Structure 3_1^- $\%\{n_1l_1j_1, n_2l_2j_2\}_\tau$
^{92}Mo	2.08	6.8	$7\%\{2d_{5/2}, 1g_{9/2}\}_\nu$ $89\%\{1g_{9/2}, 1g_{9/2}\}_\pi$	3.42	25.6	$70\%\{1g_{9/2}, 2p_{3/2}\}_\pi$ $12\%\{1g_{9/2}, 1f_{5/2}\}_\pi$
^{94}Mo	1.20	6.9	$66\%\{2d_{5/2}, 2d_{5/2}\}_\nu$ $23\%\{1g_{9/2}, 1g_{9/2}\}_\pi$	3.19	30.1	$9\%\{1h_{11/2}, 2d_{5/2}\}_\nu$ $60\%\{1g_{9/2}, 2p_{3/2}\}_\pi$ $12\%\{1g_{9/2}, 1f_{5/2}\}_\pi$
^{96}Mo	1.22	9.2	$45\%\{2d_{5/2}, 2d_{5/2}\}_\nu$ $10\%\{3s_{1/2}, 2d_{5/2}\}_\nu$ $34\%\{1g_{9/2}, 1g_{9/2}\}_\pi$	2.95	34.0	$18\%\{1h_{11/2}, 2d_{5/2}\}_\nu$ $51\%\{1g_{9/2}, 2p_{3/2}\}_\pi$ $11\%\{1g_{9/2}, 1f_{5/2}\}_\pi$
^{98}Mo	1.27	10.8	$14\%\{2d_{5/2}, 2d_{5/2}\}_\nu$ $17\%\{3s_{1/2}, 2d_{5/2}\}_\nu$ $46\%\{1g_{9/2}, 1g_{9/2}\}_\pi$	2.76	36.4	$25\%\{1h_{11/2}, 2d_{5/2}\}_\nu$ $46\%\{1g_{9/2}, 2p_{3/2}\}_\pi$ $9\%\{1g_{9/2}, 1f_{5/2}\}_\pi$

the heavier isotopes (see table 2). The calculated structures of the QRPA quadrupole and octupole states of ^{92,94,96,98}Mo represent important fingerprints for the proton–neutron composition of the $E1$ transition between 3_1^- and 2_1^+ states. For ^{92}Mo, the main contribution to the $B(E1)$ strength comes from the proton component. The proton configurations give a contribution of $B(E1)$ strength almost three times as large as the neutron configurations. For ^{94}Mo, this situation changes due to the available neutron pair above the $N = 50$ shell closure. The contribution of the neutron and proton configurations to the $B(E1)$ strength are almost equal. In heavier isotopes, there is a slight predominance of proton components in the $E1$ transitions. This QRPA analysis within the one-phonon approximation can help us to understand the evolution of $B(E1; 3_1^- \rightarrow 2_1^+)$ values in ^{92,94,96,98}Mo. However, it should be noted that the present analysis has been made within the one-phonon approach and, consequently, represents only a rough estimate.

3.3. Cluster approach

The behavior of the $B(E1, 3_1^- \rightarrow 2_1^+)$ and $B(E3, 3_1^- \rightarrow 0_{gs}^+)$ transition strengths in the Mo isotopic chain can also be described in the cluster model of a di-nuclear system [45, 46]. The model is based on the assumption that cluster-type shapes are produced by the motion of the nucleus in the mass asymmetry degree of freedom. The nuclear wavefunction can be thought of as a superposition of a mononucleus (spherical or quadrupole-deformed) and various cluster components. The weight of the various components is determined by solving the Schrödinger equation in the mass asymmetry coordinate. The contribution of cluster configurations provides a source of reflection asymmetric deformation and leads to an appearance of low-lying negative parity states. The strength of both dipole and octupole transitions is also determined by the weights of the cluster components in the wavefunctions. At the same time, the dipole transitions are very sensitive to the proton–neutron (Z/N) ratios in the clusters [47]. Previously, only the mass asymmetry was considered as an independent variable. The Z/N

ratio in the light fragment was set equal to unity, as encountered for an α particle. In order to describe the peculiarities of the $B(E1)$ strength along the isotopic chain one has to introduce charge asymmetry as an independent degree of freedom as well. This work is currently in progress.

Qualitatively, in the cluster approach the behavior of $B(E1)$ and $B(E3)$ can be explained as follows. For ^{94}Mo, the reflection asymmetric deformation originates mainly from the contribution of the ^{90}Zr+^{4}He di-nuclear system, which consists of two doubly-magic clusters. Adding neutrons while moving along the isotopic chain will lead to the decrease of the energies of the cluster systems and thus to the increase of their weight in the intrinsic wavefunction. As a result the energy of the 3^- state decreases, while the $B(E3)$ strength increases from ^{94}Mo to ^{100}Mo. For $A > 94$, the cluster contribution considered alone can be roughly represented as a core, which consists of ^{90}Zr+^{4}He, and valence neutrons moving in a field created by this core. These neutrons will act to equalize the Z/N ratio in the fragments. Therefore, although the weight of the cluster components increases along the isotopic chain, the strength of dipole transition decreases.

3.4. Comparison experiment-theory

In figure 6 the results of the calculations in the two above elucidated models are compared to the experimental values. The overall agreement of the excitation energies for the first 3^-_1 level (part (a)) is quite satisfactory and the experimental trend is well reproduced. For the values obtained using the FRSA one has to consider the influence of the neglected coupling between one- and two-phonon states (see, e.g. in [42, 48]), which, if considered, would lower the energies of the 3^-_1 levels. Another point to highlight is the validity of the FRSA for the QRPA calculations. The latter is determined by the spherical symmetry that is imposed on the quasiparticle wavefunctions and this assumption is not exactly valid for the heavier Mo isotopes. In terms of the $B(E3, 3^-_1 \rightarrow 0^+)$ strength again both models reproduce the upsloping trend. However, despite that both models reproduce the reduction in $B(E1, 3^-_1 \rightarrow 2^+_1)$ strength, they fail to reproduce the drastic decrease observed for ^{96}Mo. The variation of the effective charges in the QRPA results only in minor changes for the $E1$ strength, which allows the conclusion that the observed reduction of $E1$ strength has its origin in the structure of the wavefunctions. As mentioned earlier, the smooth evolution of the $E_{3^-_1}$ and $B(E3)$ observable indicate a rather gradual change for the ground state as well as the 3^- level. The same is indicated by the $E_{2^+_1}$ and $B(E2)$ values (e.g. see figure 1 in [10]). However, the drastic reduction in $E1$ strength for this particular transition connecting these basic building blocks of nuclear structure demonstrates the sensitivity of $E1$ transitions for small parts of the involved wavefunctions. The drastic reduction from ^{94}Mo to ^{96}Mo and near constance of this particular $E1$ value for the heavier stable isotopes highlights the difference in the involved wavefunctions of ^{96}Mo and the near-spherical ^{94}Mo but also the similarities of ^{96}Mo and ^{98}Mo. This finding indicates the similar structure of ^{96}Mo and ^{98}Mo as claimed in [7, 10]. Very likely it is the emerging γ softness in these nuclei that causes the $3^-_1 \rightarrow 2^+_1$ $E1$ strength to drop that drastically. At present both employed models do not consider this degree of freedom and future work is demanded. In order to clarify the degree of γ softness in ^{96}Mo a Coulomb-excitation analysis of excited levels as done for ^{100}Mo [49] employing the Kumar–Cline sum rules [50] is necessary.

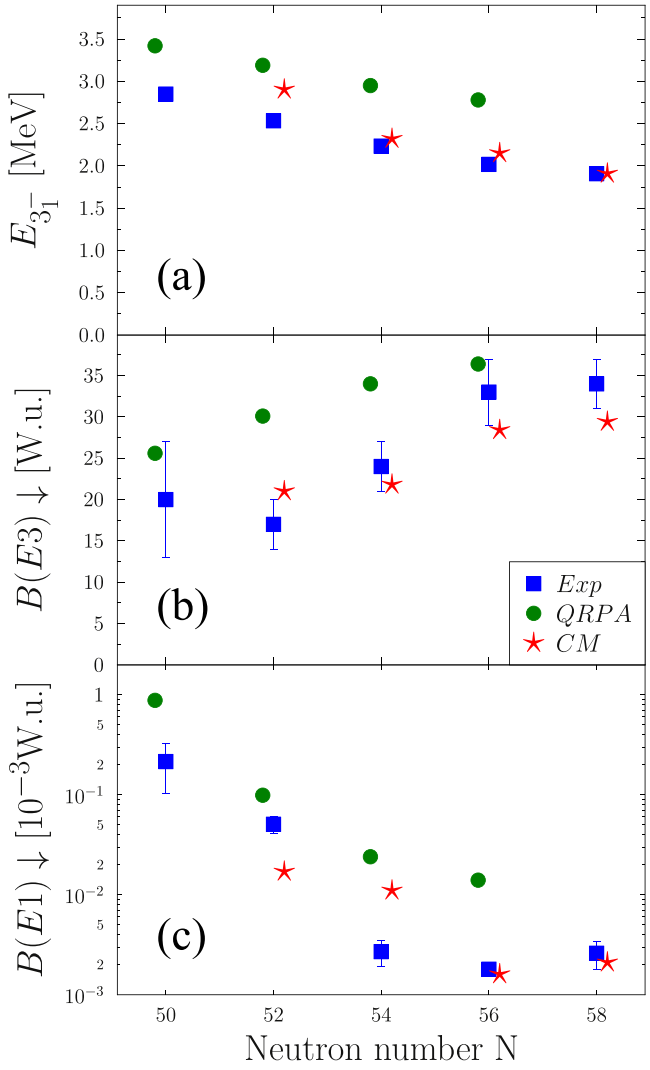

Figure 6. Comparison of experimental and calculated excitation energies and decay strengths of the first excited 3_1^- level in the stable even–even Mo isotopes. Experimental values (see figure 5) are given as (blue) squares, values calculated within the quasiparticle random phase approximation (QRPA) framework as (green) circles, and values calculated within the cluster approach (CM) as (red) stars. The excitation energies $E_{3_1^-}$ are shown in part (a). Part (b) contains the evolution of $B(E3, 3_1^- \rightarrow 0^+)$ strength and in part (c) the $B(E1)$ strength for the $3_1^- \rightarrow 2_1^+$ transition is shown in a logarithmic scale. Please note, for clarity of the presentation, the theoretical values are slightly offset from their true x-axis values.

3.5. Decay to the low-lying quadrupole isovector level

The 2_4^+ level has been identified [32] as the low-lying quadrupole isovector (mixed-symmetry) 2_{iv}^+ state. In this work, the $3_1^- \rightarrow 2_4^+$ decay has been observed and its strength determined to be $B(E1, 3_1^- \rightarrow 2_{iv}^+) = 0.27(9) \times 10^{-3}$ W.u. In comparison to ^{94}Mo ($B(E1, 3_1^- \rightarrow 2_{iv}^+) = 1.31(21) \times 10^{-3}$ W.u.) [23] this value is a factor of five weaker. For ^{98}Mo the $2_{iv}^+ \rightarrow 3_1^-$ decay from the isovector 2_{iv}^+ level at 2206 keV [51] to the 3_1^- level at 2107 keV has not been observed. Nevertheless, for ^{96}Mo the ratio R_{E1}:

$$R_{E1} = \frac{B(E1, 3_1^- \rightarrow 2_{iv}^+)}{B(E1, 3_1^- \rightarrow 2_1^+)} \tag{7}$$

of $R_{E1} = 98(12)$ is far more pronounced than the $R_{E1} = 26.0(7)$ for ^{94}Mo. Both previous values were calculated from the experimental branching ratio. As outlined in [23], in the IBM-2, the observed ratio R_{E1} can be linked to the ratio $r_\alpha = \alpha_\nu/\alpha_\pi$ of effective neutron α_ν and proton α_π boson charges:

$$r_\alpha = \frac{1 - \sqrt{R_{E1}(N_\pi/N_\nu)}}{1 + \sqrt{R_{E1}(N_\nu/N_\pi)}}. \tag{8}$$

Here, N_ν is the number of neutron bosons and N_π is the number of proton bosons. Considering ^{100}Sn as an inert core the boson numbers are $N_\nu = 2$ and $N_\pi = 4$, respectively. Therefore, r_α is calculated to $r_\alpha = -1.65(21)$, which is comparable to the values given in table 2 in [23]. The negative sign between the effective charges reflects the isovector nature of the $E1$ operator. Assuming that the decrease of $3_1^- \rightarrow 2_1^+$ strength is due to the emerging γ softness, the evolution of the R_{E1} ratio in the Mo isotopic chain, which are at least in the same order of magnitude, indicates that the isovector level is less affected by the γ softness than the isoscalar first 2_1^+ level.

4. Summary

In this contribution the lifetime of the 3_1^- level in ^{96}Mo was extracted from the known $B(E3, 3_1^- \rightarrow 0^+)$ strength and the newly measured ground-state branching ratio of the 3_1^- level. This lifetime was used to calculate the E1-decay rates, which were compared to the E1-decay rates of the 3_1^- levels in the other stable even–even Mo isotopes. A drastic reduction of the $B(E1, 3_1^- \rightarrow 2_1^+)$ strength is obvious.

Both employed theoretical models, the QRPA based FRSA as well as the cluster model reproduce the drop in the $B(E1, 3_1^- \rightarrow 2_1^+)$ strength along the Mo isotopic chain. However, the QRPA approach deviates significantly for the heavier isotopes and the cluster approach reproduces the drop, but for ^{98}Mo and not as experimentally observed for ^{96}Mo. Furthermore, the isovector $E1$ strength is reduced compared to the near-spherical neighboring isotope ^{94}Mo. However, the ratio $B(E1, 3_1^- \rightarrow 2_{iv}^+)/B(E1, 3_1^- \rightarrow 2_1^+)$ of the E1-decay strength to the low-lying quadrupole isovector (mixed-symmetry) level and the E1-decay strength to the first excited 2_1^+ level is the strongest ever observed. The observations point towards a pronounced softness in the γ degree of freedom, which was not considered in the calculations.

Acknowledgments

The authors want to highlight the financial and logistic support by the Institut Laue-Langevin to realise the fantastic opportunity of the EXILL setup. The UWS authors gratefully

acknowledge financial support by UK-STFC. MT and TK acknowledge financial support by the Deutsche Forschungsgemeinschaft (Grant No.). NNA is grateful for support by the Heisenberg-Landau program, the RFBR under Grant No. 16-52-150003 and No. 16-02-00228. TMS acknowledges the support from the RFBR and Russian Government Subsidy Program of the Competitive Growth of Kazan Federal University. NNA and TMS thank A P Severyukhin and R V Jolos for useful discussions.

ORCID iDs

M Scheck https://orcid.org/0000-0002-9624-3909

References

[1] Bohr A and Mottelson B R 1975 *Nuclear Structure* vol 2 (New York, Amsterdam: W. A. Benjamin Inc.)
[2] Garrett P E and Wood J L 2010 *J. Phys. G: Nucl. Part. Phys.* **37** 064028
[3] Stuchberry A E, Chamoli S K and Kibédi T 2016 *Phys. Rev.* C **93** 031302(R)
[4] Heyde K and Wood J L 2011 *Rev. Mod. Phys.* **83** 1467
[5] Togashi T *et al* 2016 *Phys. Rev. Lett.* **117** 172502
[6] Kremer C *et al* 2016 *Phys. Rev. Lett.* **117** 172503
[7] Thomas T *et al* 2016 *Nucl. Phys.* A **947** 203
[8] Nomura K, Rodriguez-Guzman R and Robledo L M 2016 *Phys. Rev.* C **94** 044314
[9] Gregor E T *et al* in preparation
[10] Gregor E T *et al* 2017 *Eur. Phys. J.* A **53** 50
[11] Kibédi T and Spears R H 2002 *At. Data Nucl. Data Tables* **80** 35
[12] Iskra Ł W *et al* 2018 *Phys. Lett.* B **788** 396
[13] Butler P A and Nazarejewicz W 1996 *Rev. Mod. Phys.* **68** 349
[14] Walz C *et al* 2011 *Phys. Rev. Lett.* **106** 062501
[15] Ponomarev V *et al* 1998 *Nucl. Phys.* A **635** 470
[16] Alder K and Winther A 1966 *Coulomb Excitation* (New York: Academic)
[17] Martin M J 2007 *Nucl. Data Sheets* **108** 1583
[18] Khazov Y, Rodionov A and Shulyak G 2016 *Nucl. Data Sheets* **136** 163
[19] Pietralla N 1999 *Phys. Rev.* C **59** 2941
[20] Andrejtscheff W *et al* 2001 *Phys. Lett.* B **506** 239
[21] Fransen C *et al* 2004 *Phys. Rev.* C **70** 044317
[22] Iachello F and Arima A 1987 *The Interacting Boson Model* (Cambridge: Cambridge University Press)
[23] Pietralla N *et al* 2003 *Phys. Rev.* C **68** 031305
[24] Kneissl U, Pietralla N and Zilges A 2006 *J. Phys. G: Nucl. Part. Phys.* **32** R217
[25] Pietralla N, von Brentano P and Lisetskiy A F 2008 *Prog. Part. Nucl. Phys.* **60** 225
[26] Heyde K, von Neumann Cosel P and Richter A 2010 *Rev. Mod. Phys.* **82** 2365
[27] Heyde K and Sau J 1986 *Phys. Rev.* C **33** 1050
[28] Jolos R V, Shirikova N Y and Voronov V V 2004 *Phys. Rev.* C **70** 054303
[29] Pietralla N *et al* 1994 *Phys. Rev. Lett.* **73** 2962
[30] Pietralla N *et al* 1995 *Phys. Lett.* B **349** 1
[31] Abriola D and Sonzogni A A 2008 *Nucl. Data Sheets* **109** 2501
[32] Lesher S R *et al* 2007 *Phys. Rev.* C **75** 034318
[33] Barette J *et al* 1972 *Phys. Rev.* C **6** 1339
[34] Jentschel M *et al* 2017 *J. Instrum.* **12** P11003
[35] Bernards C *et al* 2011 *Phys. Rev.* C **84** 047304
[36] Jolie J *et al* 2015 *EPJ Web Conf.* **93** 01014
[37] Heck D *et al* 1970 *Nucl. Phys.* A **159** 49
[38] Nica N, Cameron J and Singh B 2012 *Nucl. Data Sheets* **113** 1
[39] Fagg L W and Hanna S S 1959 *Rev. Mod. Phys.* **31** 711
[40] Van Giai N, Stoyanov C and Voronov V V 1998 *Phys. Rev.* C **57** 1204

[41] Severyukhin A P, Voronov V V and Van Giai N 2008 *Phys. Rev.* C **77** 024322
[42] Severyukhin A P, Arsenyev N N and Pietralla N 2012 *Phys. Rev.* C **86** 024311
[43] Lesinski T, Bennaceur K, Duguet T and Meyer J 2006 *Phys. Rev.* C **74** 044315
[44] Terasaki J *et al* 2005 *Phys. Rev.* C **71** 034310
[45] Shneidman T M *et al* 2003 *Phys. Rev.* C **67** 014313
[46] Shneidman T M *et al* 2011 *Eur. Phys. J.* A **47** 34
[47] Shneidman T M *et al* 2015 *Phys. Rev.* C **92** 034302
[48] Severyukhin A P, Voronov V V and Van Giai N 2004 *Eur. Phys. J.* A **22** 397
[49] Wrzosek-Lipska K *et al* 2012 *Phys. Rev.* C **86** 064305
[50] Cline D 1986 *Annu. Rev. Nucl. Part. Sci.* **36** 683
[51] Thomas T *et al* 2013 *Phys. Rev.* C **88** 044305